Available online at www.sciencedirect.com
SCIENCE DIRECT®
Acta Materialia 53 (2005) 4087–4095
Acta MATERIALIA
www.actamat-journals.com

Analysis of shear banding in metallic glasses under bending

Guruswami Ravichandran [a,*], Alain Molinari [b]

[a] Graduate Aeronautical Laboratories, California Institute of Technology, Pasadena, CA 91125, USA
[b] Laboratoire de Physique et Mécanique des Matériaux, Université Paul Verlaine, Ile du Saulcy, 57045 Metz Cedex 01, France

Received 17 June 2004; received in revised form 1 May 2005; accepted 8 May 2005
Available online 22 June 2005

Abstract

An analytical model is proposed for studying the formation of shear bands in metallic glasses over a wide range of size scales when subjected to plane strain bending. The model is based on elasto-plastic beam bending and the evolution of shear offset in shear bands. The spacing of shear bands is assumed to be governed by a scaling law depending on a non-dimensional material parameter which is determined from experiments. The macroscopic inelastic deformation due to bending is thought to be accommodated by slip along shear bands. The model is based on comparison of the energy dissipated along shear bands with the macroscopic dissipation obtained from the elasto-plastic theory of beam bending. The model is able to capture the following experimentally-observed scaling laws: (i) for a given thickness, the shear band spacing varies linearly with curvature; (ii) for a given curvature, the shear band offset varies as the square of the thickness; (iii) the shear band spacing varies linearly with the thickness; and (iv) failure strain (bend ductility) decreases with increasing thickness.

Keywords: Metallic glasses; Bending test; Shear bands; Ductility; Modeling

1. Introduction

Metallic glasses have been continually synthesized and investigated over the last four decades. More recently, the field of metallic glasses has gained considerable attention with the advent of the bulk metallic glasses, which have potential uses as novel structural amorphous metals [1,2]. Metallic glasses have excellent mechanical properties including high modulus, hardness, elastic limit and strength. However, they lack ductility, particularly in uniaxial tension or compression where the materials fail catastrophically by the formation of a single dominant shear band. It has been recognized that the mechanism of inelastic deformation in metallic glasses is through the formation of shear bands, which provide them with limited ductility [2,3]. These materials exhibit ductility under highly confined conditions as a result of multiplicity in shear bands, which accommodate deformation without catastrophic failure [4]. It has long been well known that thin wires or ribbons (~50 μm diameter or thickness) of metallic glasses can be bent without failure to large curvatures with the radius of curvature approximately that of the wire diameter [5–8]. However, as the diameter or thickness increases, the curvature to which the material can be bent decreases considerably and eventually thicker rods/plates (>1 mm) exhibit virtually no ductility. Understanding and quantifying this size effect is an important step towards the development of novel microstructures in metallic glasses such as foams [9] and composites [10] and as well as for design and analysis of structures made of these materials.

Recently, a series of systematic experiments were carried out by Conner et al. [11], in which they bent beams made of metallic glass, Vitreloy 106 ($Zr_{57}Cu_{15.4}Ni_{12.6}Al_{10}Nb_5$) and of various thicknesses around mandrels of different radius (0.5–3 mm). They documented a

* Corresponding author. Tel.: +1 626 395 4525; fax: +1 626 449 6359.
E-mail address: ravi@caltech.edu (G. Ravichandran).

1359-6454/$30.00
doi:10.1016/j.actamat.2005.05.011

number of seminal observations regarding the phenomena of shear banding in metallic glasses under bending as well as a number of qualitative and quantitative observations regarding shear band spacing, offset and failure. An example of the shear pattern formation in a 1.04 mm thick Vitreloy 106 sample that was bent around a mandrel of radius 3 mm is shown in the form of a scanning electron micrograph in Fig. 1. Note the nearly-evenly-spaced shear bands as well as the shear offsets at the free surface.

Conner et al. [12] have performed an analysis of the shear band formation and failure by treating the shear bands as mode II cracks. They provide a compilation of data for the failure strain (ductility) as a function of thickness of the beam for Vitreloy 1 ($Zr_{41.2}Ti_{13.8}Cu_{12.5}Ni_{10.0}Be_{22.5}$) or similar compositions. Based on their fracture mechanics analysis, they were able to explain some of the experimentally-observed features. However, a quantitative comparison with experimental data was not undertaken and the model was not able to capture the essential details of the shear banding phenomena during bending of beams or wires.

An analytical model is presented in Section 2 based on

(i) a macroscopic elasto-perfectly plastic plane strain beam bending theory with Tresca yield criterion,
(ii) a comparison of the energy dissipated along shear bands with the macroscopic dissipation calculated with theory (i).

At the macroscopic level, metallic glasses behave like elasto-perfectly plastic materials [2,12]. This feature is compatible with shear banding as a mechanism of inelastic deformation if the shear stress for which slip is activated along shear bands does not evolve with deformation until a critical failure condition is reached.

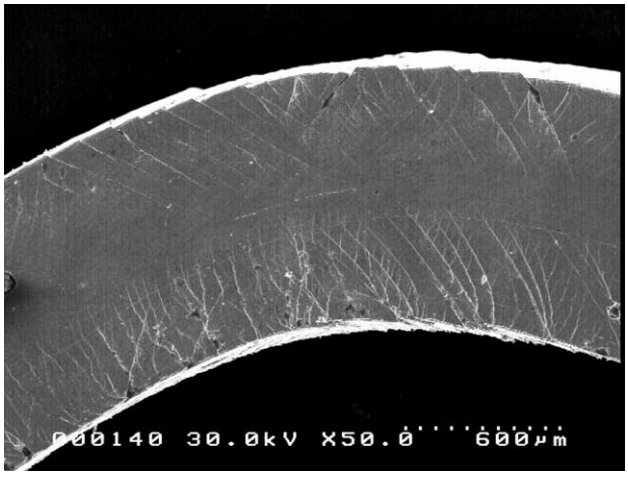

Fig. 1. Scanning electron micrograph of Vitreloy 106 (1.04 mm thick) sample bent around 2 mm radius. Note the periodic shear band pattern and the shear offset at the free surface. Micrograph courtesy of R.D. Conner and W.L. Johnson, California Institute of Technology.

The spacing of shear bands is assumed to be governed by a scaling law depending on a non-dimensional material parameter motivated by experimental observations. This approach provides closed form analytical results for the spacing of shear bands and bend ductility that are dependent on material parameters such as the Young's modulus, Poisson ratio, yield stress and the thickness of the beam. An expression for the shear displacement in the shear band is derived based on the kinematics of beam bending in the elasto-plastic range. The results shed light on the key observation for metallic glasses subjected to bending: *why do very thin wires or beams exhibit considerable ductility while thick rods/beams show relatively little ductility?* The results are correlated with available experimental data and are used to illustrate the general nature of the scaling laws in Section 3. The conclusions for the study, the limitations of the current model and potential extensions for studying failure in other geometries are discussed in Section 4.

2. Model

2.1. Elasto-plastic beam bending

The initiation, growth and failure of shear bands in metallic glasses under plane strain bending is modeled by considering an initially straight beam of unit length and rectangular cross-section with thickness h, and width, b, Fig. 2(a) and (b). The experiments considered here are for thin plates ($b \gg h$), for which plane strain conditions prevail. The stress–strain (constitutive) behavior of metallic glass is assumed to be elastic-perfectly plastic, which is consistent with the behavior of the material under uniaxial tension or compression [2,12]. The material has a Young's modulus, E, Poisson ratio, ν, and yield stress, σ_0 under uniaxial tension or compression. The material is assumed to obey isotropic Tresca yield criterion, $\sup_{i,j}|\sigma_i - \sigma_j| - \sigma_0 = 0$, where σ_i are the principal stresses ($i,j = 1,2,3$). Choosing Tresca in place of von Mises criterion allows us to simplify the analytical treatment without restricting the physical insight. Although it is known that hydrostatic pressure has an effect on the material response of metallic glasses [4], this effect will not be taken into account in the present modeling.

One-dimensional simple (Bernoulli–Euler) beam theory is employed. It is assumed that plane cross-sections remain plane and normals to neutral axis remain normal during deformation. Only infinitesimal deformations are considered and hence small strain theory is employed.

The components of the stress and strain tensors are given in the frame Oxyz of Fig. 2 by

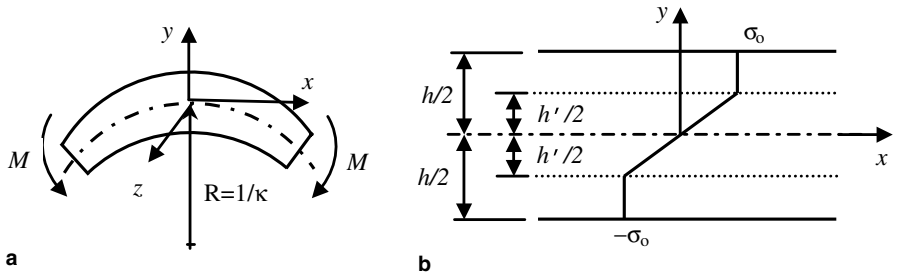

Fig. 2. (a) Schematic of a beam under plane strain bending. (b) Stress state in the cross-section of the beam beyond yield.

$$\sigma = \begin{bmatrix} \sigma_{xx} & 0 & 0 \\ 0 & 0 & 0 \\ 0 & 0 & \sigma_{zz} \end{bmatrix}, \quad \varepsilon = \begin{bmatrix} \varepsilon_{xx} & 0 & 0 \\ 0 & \varepsilon_{yy} & 0 \\ 0 & 0 & 0 \end{bmatrix} \tag{1}$$

with $\sigma_{yy} = 0$ by assuming stress free boundaries conditions at $y = \pm h/2$, and $\varepsilon_{zz} = 0$ from the plane strain assumption. In the elementary beam theory, the total axial strain (ε_{xx}) varies linearly in the thickness direction (y):

$$\varepsilon_{xx} = \kappa y, \tag{2}$$

where y is measured from the neutral axis (Fig. 2(a)). κ is the current curvature of the beam and is related to the radius of curvature, R through simple relation, $\kappa = 1/R$.

The sign convention for curvature (κ) is chosen such that it is positive for the deformed beam shown in Fig. 2(a). Also, tensile stresses and strains are assumed to have the positive sign. The origin of the coordinate axes for the beam is chosen so as to coincide with the neutral axis ($y = 0$). The beam is assumed to bend in a symmetric fashion such that the neutral axis lies along $y = 0$ at all stages of deformation.

During elastic loading of the beam, the stress field has the form

$$\sigma_{xx} = E'\varepsilon_{xx}, \quad \sigma_{zz} = \nu\sigma_{xx} \quad \text{with } E' = \frac{E}{1-\nu^2}. \tag{3}$$

Upon increasing the bending moment or the curvature, the outer fibers ($y = \pm h/2$) of the beam reach, according to Tresca criterion, the yield stress $\sigma_{xx} = \pm\sigma_0$ at the strain $\varepsilon^0_{xx} = \pm\sigma_0/E'$ for the curvature κ_0

$$\kappa_0 = \frac{2\sigma_0}{E'h}. \tag{4}$$

As the bending moment (curvature) is further increased beyond yield curvature, the elastic–plastic boundary moves towards the neutral axis. The location of the elastic plastic boundary ($y = \pm h'/2$) can be determined as

$$h' = \frac{2\sigma_0}{E\kappa}. \tag{5}$$

Note that the regions, $|y| > h'/2$ are the "*plastic zones*" of the beam.

Using the stress–strain relation, the stress and strain distribution in the beam can be written as

$$\begin{aligned} &\sigma_{xx} = E'\kappa y, \quad \sigma_{zz} = \nu E'\kappa y, \quad \varepsilon_{xx} = \kappa y = \sigma_{xx}/E', \\ &\varepsilon_{yy} = -\frac{\nu}{(1-\nu)E'}\sigma_{xx} \quad \text{for } |y| \leqslant h'/2, \end{aligned} \tag{6}$$

$$\sigma_{xx} = \sigma_0, \quad \sigma_{zz} = \nu\sigma_0 \quad \text{for } h'/2 \leqslant y \leqslant h/2, \tag{7a}$$

$$\begin{aligned} &\varepsilon_{xx} = \kappa y = \frac{\sigma_0}{E'} + \varepsilon^{\mathrm{p}}_{xx}, \\ &\varepsilon_{yy} = -\frac{\nu}{(1-\nu)E'}\sigma_0 - \varepsilon^{\mathrm{p}}_{xx} \quad \text{for } h'/2 \leqslant y \leqslant h/2, \end{aligned} \tag{7b}$$

where $\varepsilon^{\mathrm{p}}_{xx}$ is the axial plastic strain. In the lower plastic zone σ_0 is changed into $-\sigma_0$ in (7). Note that plastic deformations are of the form

$$\varepsilon^{\mathrm{p}}_{xx}, \quad \varepsilon^{\mathrm{p}}_{yy} = -\varepsilon^{\mathrm{p}}_{xx}, \quad \varepsilon^{\mathrm{p}}_{zz} = 0. \tag{8}$$

The state of stress across the undeformed cross-section of the beam for deformation beyond yield is illustrated in Fig. 2(b).

2.2. Shear banding

From the experimental work of Conner et al. [11] and of others cited therein, the initiation and growth of shear bands in beams made of metallic glasses subjected to pure bending can be modeled as follows. All the shear bands are assumed to initiate at the external boundaries of the beam ($|y| = h/2$) when the strain at these locations reach the yield strain (ε^0_{xx}). It is recognized that the shear band is present only in the plastically deforming region $|y| \geqslant h'/2$.

Two systems of shear bands with distinct width and orientations are apparent in Fig. 1. Shear bands of system (I) are called "primary shear bands" and have larger band width and spacing than those of system (II). They grow inwards towards the neutral axis at an angle 45% to the vertical axis as shown in Fig. 3(a). The shear bands considered here are assumed to terminate at the elastic plastic boundary. The system (II) of "secondary shear bands" has smaller band width and spacing. The difference in the morphology and patterning of shear bands can be attributed to the asymmetry of the forming

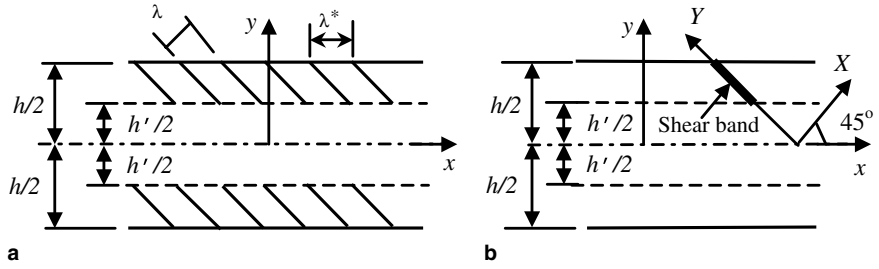

Fig. 3. (a) Schematic of the primary shear band pattern with uniform spacing λ ($\lambda^* = \sqrt{2}\lambda$ is the spacing measured by Conner et al. [11]). (b) Geometry and coordinates for a single shear band in the tensile region of the beam. Note that two conjugate families of shear bands with angles ±45° (with respect to the neutral axis) may contribute to the overall inelastic deformation, but, for clarity of the figure, only one has been displayed.

process and friction effects. The samples were clamped at one end with a die brake and bent around a mandrel of constant radius. If the experiments were conducted by clamping the other end and bending in the reverse direction, the shear band systems would be exchanged as (I) → (II) and (II) → (I).

A visualization of the configuration of shear band (I) was introduced by Conner et al. [12]. They analyzed these shear bands by treating them as mode II (inplane shear) cracks, which is equivalent to treating the shear bands with discontinuities in the tangential displacement. In this approach, fracture mechanics considerations were used for explaining the observed shear band spacing, offset and failure strain of metallic glasses. However, it is well known that shear bands can sustain stress and have a gradient of shear displacements within the band. In the present approach, the shear bands are treated as materials with strength that can sustain considerable inelastic shear deformation prior to failure.

The shear displacement on the shear band boundaries can be derived from kinematic considerations. An individual shear band (I) in a beam under bending is shown in Fig. 3(b), with the associated coordinate system, X–Y, with Y-axis being in the direction along the band and X-axis being normal to the band. The X-axis makes an angle +45° with the x-axis (beam coordinate). The plastic shear strain in the XY frame can be related to the plastic strains (8) given by the beam theory

$$\varepsilon^{\mathrm{p}}_{XY} = \tfrac{1}{2}(\varepsilon^{\mathrm{p}}_{yy} - \varepsilon^{\mathrm{p}}_{xx}) = -\varepsilon^{\mathrm{p}}_{xx}. \tag{9}$$

The modeling developed here is for shear banding in the upper plastic zone. Similar considerations can be made for the lower plastic zone. The spacing λ of shear bands (I) is taken as uniform, Fig. 3(a). For a given band (I), the slip displacement δ_{I} due to plastic shearing between the two boundaries is scaled by the magnitude of the shear strain $\varepsilon^{\mathrm{p}}_{XY}$ or equivalently by $\varepsilon^{\mathrm{p}}_{xx}$,

$$\delta_{\mathrm{I}} = L\varepsilon^{\mathrm{p}}_{xx}, \tag{10}$$

where L has the dimension of length. From the beam theory we have

$$\varepsilon^{\mathrm{p}}_{xx} = \kappa y - \frac{\sigma_0}{E'} = \frac{2\sigma_0}{E'h'}\left(y - \frac{h'}{2}\right) = \kappa\left(y - \frac{h'}{2}\right). \tag{11}$$

2.3. Dissipation

For metallic glasses, the basic mechanism of inelastic deformation is shear banding [2,4]. For consistency, it is stated here that the total energy dissipated along shear bands is identical to the dissipated energy D_{BT} as calculated by the elasto-plastic Beam Theory (BT). The analysis is made for the upper part ($y \geqslant 0$) of the beam and for the unit length ($\Delta x = 1$). A similar analysis may be done for the lower part. The total dissipation due to inelastic deformation is composed of the dissipation D_{I} and D_{II} along bands (I) and (II), respectively, and of the additional dissipation D_{add} possibly due to inelastic deformations along networks of shear bands at a finer scale which are not visible in Fig. 1 (previous shear bands of type (I) which have been arrested, tertiary shear bands growing between shears bands (II), etc.). The balance of dissipated energy has the form

$$D_{\mathrm{I}} + D_{\mathrm{II}} + D_{\mathrm{add}} = D_{\mathrm{BT}}. \tag{12}$$

Considering the dissipation D_{SB} along an individual band (I), and denoting by $N_{\mathrm{SB}} = 1/(\lambda\sqrt{2})$ the number of bands (I) per unit length of beam, we have,

$$D_{\mathrm{I}} = N_{\mathrm{SB}} D_{\mathrm{SB}}. \tag{13}$$

From Tresca criterion, the slip resistance is $\tau_0 = \sigma_0/2$, and therefore,

$$D_{\mathrm{SB}} = b\int_{h'/\sqrt{2}}^{h/\sqrt{2}} \tau_0 \delta_{\mathrm{I}}(Y)\,\mathrm{d}Y = \frac{\sqrt{2}}{8} L \frac{\sigma_0^2 b}{E'h'}(h - h')^2, \tag{14}$$

where (10) and (11) have been used. Finally, (13) takes the form

$$D_{\mathrm{I}} = \frac{L}{\lambda}\tilde{D} \tag{15}$$

with

$$\tilde{D} = \frac{1}{8}\frac{\sigma_0^2 b}{E'h'}(h - h')^2. \tag{16}$$

From the macroscopic point of view, the total dissipation D_{BT} may be evaluated by considering the plastic beam theory. At a given point, the plastic work per unit volume $\int_0^t \sigma_{ij}\dot{\varepsilon}^p_{ij}\,dt$ can be written as $\sigma_0\varepsilon^p_{xx}$ by taking account of $\sigma_{xx} = \sigma_0$ in the plastic zone, and of $\sigma_y = 0$, $\dot{\varepsilon}^p_{zz} = 0$ at any point. Considering that, for a perfectly plastic material the plastic work is entirely dissipated, the dissipation in the upper plastic zone is

$$D_{BT} = \int_{y\geqslant 0} \sigma_0\varepsilon^p_{xx}\,dV = b\sigma_0\int_{h'/2}^{h/2} \varepsilon^p_{xx}(y)\,dy = 2\tilde{D}. \tag{17}$$

From (12), we have the following inequality:

$$D_I \leqslant D_{BT}, \tag{18}$$

which by substitution of (15) and (17) provides the following upper bound estimates of L and of the slip displacement:

$$L \leqslant 2\lambda, \quad \delta_I \leqslant \delta_I^{UP}, \tag{19}$$

where

$$\delta_I^{UP} = 2\lambda\varepsilon^p_{xx} = 2\lambda\kappa\left(y - \frac{h'}{2}\right). \tag{20}$$

Upper bounds are effectively obtained by assuming that the dissipation along shear bands other than (I) is negligible. In other words, the upper bound results can also be viewed as a model where inelastic deformation is mainly due to shear bands (I).

The step size or the shear displacement of a primary shear band has been measured and documented by Conner et al. [11] as the shear offset. The shear offset (Δ) is measured after unloading following elasto-plastic bending, and, approximates to first order, the plastic part of the shear displacement evaluated at the surface, $y = h/2$, with the model (20),

$$\Delta = \lambda\kappa(h - h') = \lambda\kappa\left(h - \frac{2\sigma_0}{E'\kappa}\right). \tag{21}$$

2.4. Shear band spacing

Since metallic glasses are amorphous and do not possess microstructure, there is no material length scale in the problem to suggest a scaling law for the shear band spacing λ.

However, experimental data show that, for a given curvature, the shear band offset varies as the square of the thickness. Since shear banding is a mechanism of inelastic deformation taking place within the plastic zone, it is appealing to restitute the square dependence of Δ upon the thickness h by scaling the shear band spacing with the plastic zone size, $(h - h')/2$,

$$\lambda = \alpha(h - h'), \tag{22}$$

where α is a non-dimensional proportionality parameter, which may be material dependent. Thus, we have

$$\Delta = \alpha\kappa(h - h')^2 = \frac{2\alpha\sigma_0}{E'h'}(h - h')^2. \tag{23}$$

The spacing of primary shear bands can be written as

$$\lambda = \alpha(h - h') = \frac{2\alpha\sigma_0}{E'}\left(\frac{1}{\kappa_0} - \frac{1}{\kappa}\right) = \frac{2\alpha\sigma_0}{E'}(R_0 - R) \tag{24}$$

and the number of primary shear bands in the upper plastic zone, per unit length of beam, is,

$$N_{SB} = \frac{1}{\lambda\sqrt{2}} = \frac{1}{\sqrt{2}\alpha(h - h')} = \frac{1}{2\sqrt{2}}\frac{E'}{\alpha\sigma_0}\left(\frac{1}{\kappa_0} - \frac{1}{\kappa}\right)^{-1}. \tag{25}$$

Eq. (24) provides a simple analytical expression for the shear band spacing in terms of the material and geometrical parameters. The shear band spacing scales linearly with the plastic zone size of the beam. Equivalently, the shear band spacing is linearly proportional to the difference in the radii of curvature at yield (R_0) and the current value (R). The effect of material properties enters through the ratio of the yield stress to the modified Young's modulus $E' = E/(1 - \nu^2)$. It is also noted that the number of shear bands per unit length and the shear band spacing are not constant but are functions of deformation, namely the current curvature of the beam. The values for shear band spacing are not generally available as a function of deformation (curvature). The limited data available in the literature confirms the scaling law shown in (24) for the shear band spacing [11].

It is worth noting that, all other parameters being fixed, the number of shear bands (I) increases for larger values of the Poisson ratio, according to the definition of the modified Young's modulus, E'.

2.5. Failure criterion

The data for shear band spacing and offset have been compiled by Conner et al. [11,12] over a wide range of wire, rod and beam sizes at or near failure of the material. Note that those data concern primary shear bands. In order to make direct comparisons with the experimental data, it becomes necessary to invoke a failure criterion. It has been noted by Conner et al. [12] that failure of beams of metallic glass is associated with a critical shear offset. Based on this observation, when the plastic shear band displacement at the boundary (23) reaches the critical value for the shear offset, failure is said to occur. The corresponding deformation (curvature, κ_c) and the location of the elastic plastic boundary ($y = h'_c/2$) can be used to characterize the shear band spacing (λ_c) and as well as the ductility or failure strain in bending. The failure criterion can now be expressed using (23) as

$$\Delta_c = \frac{2\alpha\sigma_0}{E'h'_c}(h - h'_c)^2. \tag{26}$$

Once the critical shear offset is used as a failure criterion, (26) can be viewed as an algebraic equation for h'_c, the location of the elastic–plastic boundary at failure. By denoting, $H'_c = h'_c/h$, (26) can be written in a non-dimensional form as

$$\frac{E'\Delta_c}{2\alpha\sigma_0 h}H'_c = (1 - H'_c)^2. \tag{27}$$

A non-dimensional parameter a (>0) is introduced for the purpose of analysis

$$a = \left(\frac{E'}{\sigma_0}\right)\left(\frac{\Delta_c}{4\alpha h}\right). \tag{28}$$

Recall that α is an undetermined non-dimensional material constant and could be viewed as a scaling parameter for the characteristic length, with typical values between 0 and 1.

The physically relevant solution to the quadratic equation (27) can be expressed in terms of the non-dimensional parameter a

$$H'_c = \frac{h'_c}{h} = \frac{\kappa}{\kappa_c} = (1 + a) - a\sqrt{1 + \frac{2}{a}}. \tag{29}$$

The shear band spacing at failure can be written in an explicit form using (24) and (29)

$$\lambda_c = \alpha h\left(1 - \frac{h'_c}{h}\right) = \alpha h a\left(\sqrt{1 + \frac{2}{a}} - 1\right). \tag{30}$$

The strain at failure (ductility) can be written as

$$\varepsilon_f = \frac{\kappa_c h}{2} = \frac{\sigma_0}{E'}\frac{h}{h'_c} = \frac{\sigma_0}{E'}\frac{1}{\left[(1 + a) - a\sqrt{1 + \frac{2}{a}}\right]}. \tag{31}$$

The expressions (30) and (31) are analytical predictions for shear band spacing at failure and failure strain of beams made of metallic glass subjected to bending based on critical shear offset failure criterion. The results are in terms of the non-dimensional parameter, a, which is function of material properties and the thickness (h) of the beam. In order to have better understanding of the shear band spacing and ductility, the expressions (30) and (31) are expanded in a Taylor series for large a ($\gg$1), which is of practical interest,

$$\lambda_c \approx \alpha h\left(1 - \frac{1}{2a}\right) = \alpha h\left(1 - \frac{2\alpha\sigma_0}{E'\Delta_c}h\right), \tag{32}$$

$$\varepsilon_f \approx 2\frac{\sigma_0}{E'}a = \left(\frac{\Delta_c}{2\alpha h}\right). \tag{33}$$

The analytical predictions show that the shear band spacing (32) scales linearly with the thickness (h) for relevant values (up to 1 mm) and is in excellent agreement with the experimental observations of Conner et al. [11]. The failure strain is shown to be inversely proportional to the thickness ($1/h$). Based on the experimental data compiled by Conner et al. [12], it was concluded that the strain to failure scales inversely with the square of the thickness, which is not in agreement with the present model. Direct comparison to experiments is performed in the next section, and the experimental observations will be discussed further in detail.

The expression for the strain to failure (33) clearly shows the reason why "thin" wires or beams can be bent severely without failure, while "thick" beams or wires lack ductility and fail in a brittle manner. In the following, a heuristic criterion is provided to distinguish between thin and thick for metallic glasses. The typical strain to failure under uniaxial compression or tension for most metallic glasses is around 0.02. It is suggested that the wire or beam could be classified such that it is said undergo ductile deformation if the strain to failure is equal or greater than 0.1. The thickness at which the transition occurs (from ductile to brittle) can be deduced from (33):

$$h^* = 10\left(\frac{\Delta_c}{2\alpha}\right). \tag{34}$$

Beams of thickness smaller than h^* would exhibit ductile behavior in bending while those with thickness larger than h^* would fail in a brittle manner. The relation (34) provides a simple way of classifying expected material behavior in terms of the material parameters, the critical shear offset (Δ_c) and the parameter α. In the next section, the results of the upper bound model are compared to experimental data. The extension of the present upper bound model to predict the spacing of the secondary shear bands is discussed in Appendix A.

3. Results

3.1. Material properties and experimental data

In order to validate the predictive capabilities of the model described in the previous section, direct comparison is made with well-documented data in the literature. For shear band spacing and the dependence of shear offset on the radius of curvature, the data provided by Conner et al. [11] for Vitreloy 106 ($Zr_{57}Cu_{15.4}Ni_{12.6}Al_{10}Nb_5$) for bending around mandrels of various radii ranging from 0.5 to 3 mm are used. In addition, for the failure strain, the data provided by Conner et al. [12] for a variety of metallic glasses including Vitreloy 1 are used for comparison. The relevant mechanical properties needed for modeling are taken from these two publications for Vitreloy 1 and Vitreloy 106 and are shown in Table 1.

3.2. Comparison with experimental data

3.2.1. Shear band spacing

The model predications for shear band spacing near failure is plotted in Fig. 4 as a solid curve using (30)

Table 1
Mechanical properties of Vitreloy 1 and Vitreloy 106, adapted from [11,12]

Property	Vitreloy 1 ($Zr_{41.2}Ti_{13.8}Cu_{12.5}$-$Ni_{10.0}Be_{22.5}$)	Vitreloy 106 ($Zr_{57}Cu_{15.4}$-$Ni_{12.6}Al_{10}Nb_5$)
Young's modulus, E (GPa)	97	86.7
Poisson's ratio, ν	0.36	0.38
Yield strength, σ_0 (MPa)	1900	1800[a]
		1200[b]

[a] Uniaxial compression.
[b] Uniaxial tension.

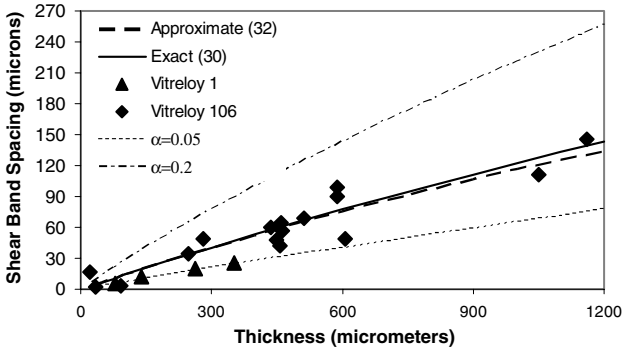

Fig. 4. Shear band spacing $\lambda_c^* = \sqrt{2}\lambda_c$ at failure as a function of thickness. Analytical predictions ($\alpha = 0.1$, $\Delta_c = 20$ μm), approximate (Eq. (32)) and exact (Eq. (30)) are shown, along with experimental data for Vitreloy 1 and Vitreloy 106. The sensitivity of predictions to the parameter α is illustrated for $\alpha = 0.05$ and 0.2.

for a value of $\alpha = 0.1$, which is the only parameter that is not obtained from independent measurements. For the purpose of comparison, we use the same measure of spacing $\lambda_c^* = \sqrt{2}\lambda_c$ as in experiments. The approximate solution given by (32) is plotted as a dashed curve and matches the exact solution for range thickness of interest in the experiments. The experimental data for Vitreloy 106 taken from Conner et al. [11] are plotted as filled symbols. The agreement between the model predictions and the experimental data is good. The prediction captures the near linearity of the experimental data and suggests a scaling for the shear band spacing of, $\lambda_c = 0.1h$, which is in fair agreement with experimental observations. The analytical predictions become non-linear for relatively large thickness ($h > 1$ mm) which needs further experimental validation. The compressive yield stress of Vitreloy 106 (1800 MPa) is used for predictions, whenever the value for σ_0 is required.

The model predictions for different values of $\alpha = 0.05$ and 0.2 are also plotted in the same Fig. 4 and show the sensitivity of the model to this parameter. It is interesting to note that the shear band spacing from the experimental data for Vitreloy 1 plotted in the figure agrees well with prediction based on $\alpha = 0.05$. In the following sections, a constant value of $\alpha = 0.1$ and critical shear offset $\Delta_c = 20$ μm are used for Vitreloy 106, unless otherwise mentioned.

3.2.2. Evolution of shear band spacing and shear offset

The evolution of shear band spacing and shear offset for a constant thickness ($h = 0.457$ mm) as a function of the radius of curvature are plotted for Vitreloy 106 in Fig. 5. As for Fig. 4, the measure $\lambda^* = \sqrt{2}\lambda$ of shear band spacing is used. The experimental data for bend radius ranging from 0.5 to 3 mm are shown as filled symbols. The agreement between the model predictions and the experimental data is good, particularly for larger radii of curvature. It is interesting to note that the shear band spacing decreases linearly with increasing radius of curvature, while the shear offset increases non-linearly with decreasing radius of curvature. The predictions for shear offset at small radii of curvature ($R < 0.5$ mm) need further experimental study.

The predictions for the shear band offset for a fixed radius of curvature (1 mm) for beams of varying thickness made of Vitreloy 106 are shown in Fig. 6. The experimental data points are shown as filled symbols.

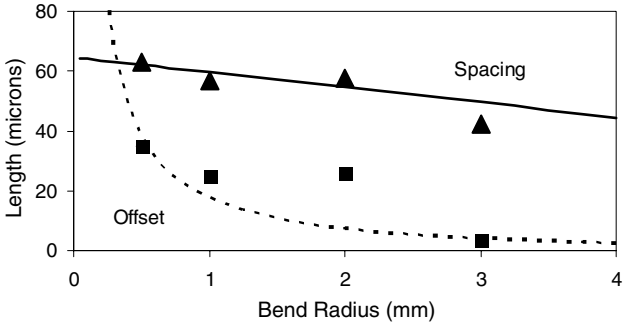

Fig. 5. Predictions of shear band spacing $\lambda^* = \sqrt{2}\lambda$ (λ given by Eq. (24)) and shear offset (Eq. (23)) for a constant thickness ($h = 0.457$ mm) beam as a function of the radius of curvature for Vitreloy 106 ($\alpha = 0.1$, $\Delta_c = 20$ μm). The experimental data [11] are shown as filled symbols.

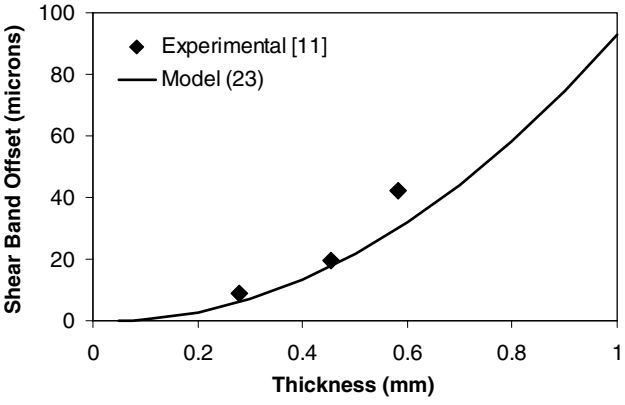

Fig. 6. Predicted shear band offset (Eq. (23)) at a fixed radius of curvature (1 mm) for beams of varying thickness made of Vitreloy 106 ($\alpha = 0.1$, $\Delta_c = 20$ μm). The experimental data [11] are shown as filled symbols.

The analytical predictions show that the shear offset increases as the square of the plate thickness, which is in agreement with experimental observations [11].

3.2.3. Failure strain

The analytical prediction for failure strain using (31) is plotted for Vitreloy 1 in Fig. 7 for the following values of the parameters, $\alpha = 0.1$ and critical shear offset $\Delta_c = 20$ μm. The value of the critical shear offset (Δ_c) was kept the same as the one for Vitreloy 106. The experimental data are shown as filled symbols with error bars and is taken from Conner et al. [12] for compositions similar to Vitreloy 1. There is fair agreement between the model and the experimental data. As has been noted earlier, the failure strain (a measure of ductility) is inversely proportional to the beam thickness. The transition thickness h^* (34) at which material ceases to be ductile is computed to be 1 mm for Vitreloy 1. This value is in good agreement with the experimental observations.

For illustrative purposes, the predictions for different values of $\alpha = 0.05$ and 0.2 are also shown in Fig. 7. It is evident that though the scaling law for the thickness holds, the failure strain is increased for smaller value of α (equivalent to larger critical shear offset), while larger value of α (equivalent to smaller critical shear offset) means smaller strain to failure. It is also interesting to note that the predicted failure strain appears to become insensitive to the value of α for very large thickness. At large thickness, the predicted failure strains are overestimated in comparison to the experimental data.

It is noted that Conner et al. [12] suggest that the failure strain scales as the inverse square of the thickness. This is based on a wide range of alloys with compositions similar to Vitreloy 1. In light of this, a careful examination of the data does not entirely support their scaling law. Detailed investigations of the dependence of the strain to failure (ductility) as a function of thickness needs to be performed for alloys of fixed composition to verify the scaling law suggested by the present model.

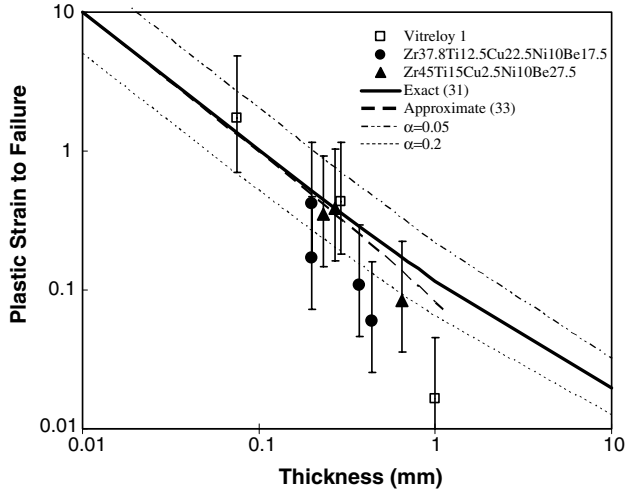

Fig. 7. Strain to failure as a function of beam thickness for Vitreloy 1 (log–log diagram). The analytical predictions ($\alpha = 0.1$, $\Delta_c = 20$ μm), exact (Eq. (31)) and approximate (Eq. (33)) are shown along with experimental data [12] for Vitreloy 1 and other similar compositions. The sensitivity of the predictions to the parameter α is illustrated for $\alpha = 0.05$ and 0.2.

4. Conclusions and discussion

A simple analytical model for studying the phenomena of shear banding in thin plates made of metallic glasses subjected to plain strain bending is presented. The model is based on one-dimensional elasto-plastic plane strain beam bending theory and the concept of shear band dissipation. This simple model is able to capture all the essential features of the experimental observations regarding shear band spacing, offset and failure strain for a variety of metallic glasses. An important parameter that plays a major role in setting the shear band spacing is the critical shear band offset which deserves further study. The model is based on simple beam theory and does not account for finite (large) deformations. The effects of boundary conditions including clamping and friction are not accounted for in the present model, which would be needed to model the shear band patterns on the compressive side of the sample. As predicted by the model, the shear band spacing does increase with increasing curvature and eventually saturates.

In deriving the expression for the shear band spacing (22), a choice of characteristic length scale was needed to be made. There are two possible choices that can be made: (i) plastic zone size ($h - h'$) and (ii) shear band thickness. In the current work, the characteristic length was chosen to be the plastic zone size and the subsequent results were derived.

It should be noted that the failure criterion is based on the critical shear offset, which needs to be characterized based on analytically tractable experiments and is not currently readily available. It is suggested here that simple torsion experiments of rods of various sizes can be expected to provide such data.

It is possible to generalize the concepts developed here to study inelastic deformation in metallic glasses of other geometries and loading, including cracks, notches and holes subjected to tension or compression, cylinders subjected to torsion, hollow cylinders and spheres subjected to internal or external pressure. In addition to data for shear band spacing and offset, it would be useful to measure load (moment) and displacement (rotation) during the experiments. Further modeling and experimentation on the type of geometries and loading suggested here and others would provide additional insight into the material behavior of metallic

glasses. This would also guide processing of novel microstructures to prevent catastrophic brittle failure commonly associated with metallic glasses.

Acknowledgments

The support for this work from the Defense Advanced Research Projects Agency (DARPA), under ARO Contract No. DAAD19-01-1-0525, with Dr. Leo Christodoulou as Program Manager is gratefully acknowledged. G.R. thanks Dr. Dale Conner and Professor William L. Johnson for insightful discussion on metallic glasses and the authors thank them for providing the micrograph in Fig. 1. G.R. acknowledges with appreciation, the hospitality provided by the Laboratoire de Physique et Mécanique des Matériaux (LPMM, UMR CNRS 7554) during his visit to the Université Paul Verlaine-Metz. A.M. acknowledges with appreciation, the hospitality provided by the Graduate Aeronautical Laboratories during his visit to the California Institute of Technology.

Appendix A. Secondary shear bands

In the upper bound model presented in the paper, the contribution of secondary shear bands to the global dissipation was neglected. Here, we discuss the combined effect of shear bands (I) and (II). Shear banding at a smaller scale (tertiary, etc.) is neglected. According to Tresca criterion, secondary shear bands should have an angle of $-45°$ with respect to the axis (y). Therefore in the present modeling, bands (I) and (II) are perpendicular. The balance of dissipated energy (12) takes the form

$$D_{\mathrm{I}} + D_{\mathrm{II}} = D_{\mathrm{BT}}. \tag{A.1}$$

Assume now that

$$D_{\mathrm{II}} = \beta D_{\mathrm{I}}, \tag{A.2}$$

where $0 \leqslant \beta \leqslant 1$ is a constant material parameter. It can be shown that the relationship (A.2) is equivalent to postulating that the total shear carried by the shear band system (II) is smaller by the factor β with respect to those carried by system (I). Using (10), (15), (17), (A.1) and (A.2), it follows that

$$L = \frac{2\lambda}{1+\beta}, \quad \delta_{\mathrm{I}} = \frac{2\lambda\kappa}{1+\beta}\left(y - \frac{h'}{2}\right). \tag{A.3}$$

Thus, using the scaling law (22), the shear displacement offset has the form

$$\Delta = \frac{\alpha\kappa}{1+\beta}(h-h')^2 = \frac{2\alpha\sigma_0}{(1+\beta)E'h'}(h-h')^2. \tag{A.4}$$

Note that the upper bound model corresponds to $\beta = 0$.

The scaling law (22) for primary shear bands can be written in terms of the length of primary shear bands as

$$\lambda = \alpha^* \frac{h-h'}{\sqrt{2}}, \tag{A.5}$$

where $\alpha^* = \sqrt{2}\alpha$.

From our model, shear bands (I) and (II) are perpendicular. Two primary shear bands are connected by segments of shear bands (II) with length λ. Assuming that bands (II) have a regular spacing λ_{II}, it is reasonable to analyze the patterning of secondary shear bands by extrapolating the scaling law (A.5), thus obtaining a hierarchical structure for the shear band patterning,

$$\lambda_{\mathrm{II}} = \alpha^* \lambda. \tag{A.6}$$

Using the value $\alpha = 0.1$ for Vitreloy 106, one obtains $\lambda_{\mathrm{II}} = 0.14\lambda$, which is roughly in agreement with the spacing associated with patterning of secondary shear bands (II) in Fig. 1. It is possible to extend this line of reasoning for predicting the spacing of tertiary and higher order shear bands.

References

[1] Inoue A. Bulk amorphous alloys: preparation and functional characteristics. Uetikon-Zuerich: Trans Tech Publications; 1998.
[2] Johnson WL. MRS Bull 1999;24:42.
[3] Pekarskaya E, Kim CP, Johnson WL. J Mater Res 2001; 16:2513.
[4] Lu J, Ravichandran G. J Mater Res 2003;18:2039.
[5] Zielinski PG, Ast DG. Philos Mag A 1983;48:811.
[6] Petouhoff NL, Ardell AJ, Jankowski AF. Acta Metall Mater 1992;40:3167.
[7] Suto S, Matsuno K, Sano T, Matsui K. J Mater Proc Technol 1992;33:215.
[8] Katuya A, Inoue A, Amiya K. Int J Rapid Solid 1996;9:137.
[9] Schroers J, Veazey C, Johnson WL. Appl Phys Lett 2003; 82:370.
[10] Hays CC, Kim CP, Johnson WL. Phys Rev Lett 2000;84:2901.
[11] Conner RD, Li Y, Nix WD, Johnson WL. Shear band spacing under bending of Zr-based metallic glass plates. Acta Mater 2004;52:2429.
[12] Conner RD, Johnson WL, Paton NE, Nix WD. J Appl Phys 2003;94:904.